Spectrochimica Acta Part A 94 (2012) 288–301

Contents lists available at SciVerse ScienceDirect

Spectrochimica Acta Part A: Molecular and Biomolecular Spectroscopy

journal homepage: www.elsevier.com/locate/saa

Molecular structure, spectral studies, intra and intermolecular interactions analyses in a novel ethyl 4-[3-(2-chloro-phenyl)-acryloyl]-3,5-dimethyl-1*H*-pyrrole-2-carboxylate and its dimer: A combined DFT and AIM approach

R.N. Singh*, Vikas Baboo, Poonam Rawat, Amit Kumar, Divya Verma

Department of Chemistry, University of Lucknow, Lucknow 226007, UP, India

ARTICLE INFO

Article history:
Received 28 November 2011
Received in revised form 18 March 2012
Accepted 22 March 2012

Keywords:
Vibrational spectrum
Dimer
Weak interaction
Intermolecular hydrogen bond
Reactivity descriptor
Ellipticity

ABSTRACT

A newly synthesized chalcone, Ethyl 4-[3-(2-chloro-phenyl)-acryloyl]-3,5-dimethyl-1*H*-pyrrole-2-carboxylate (ECPADMPC) has been characterized by ^{1}H NMR, ^{13}C NMR, UV–Vis, FT-IR, Mass spectroscopy and elemental analysis. Quantum chemical calculations have been performed by DFT level of theory using B3LYP functional and 6-31G(d,p) as basis set. The time dependent density functional theory (TD-DFT) is used to find the various electronic transitions within molecule. A combined theoretical and experimental wavenumber analysis confirms the existence of dimer. Topological parameters-electron density (ρ_{BCP}), Laplacian of electron density ($\nabla^2\rho_{BCP}$), energetic parameters-kinetic electron energy density (G_{BCP}), potential electron density (V_{BCP}) and the total electron energy density (H_{BCP}) at the bond critical points (BCP) have been analyzed by 'Atoms in molecules' AIM theory in detail. The intermolecular hydrogen bond energy of dimer is calculated as −12.3 kcal/mol using AIM calculations. AIM ellipticity analysis is carried out to confirm the presence of resonance assisted intermolecular hydrogen bonds in stabilization of dimer. The analysis clearly depicts the presence of different kind of interactions in dimer. This dimer may work as model system to understand the H-bonding interaction in biomolecules. The local reactivity descriptor analysis is performed to find the reactive sites within molecule.

1. Introduction

Chalcones are aromatic ketones that form the central core for a variety of important biological compounds. Chalcones are abundant in edible plants and work as precursors for flavonoids and isoflavonoids [1]. They have relatively low redox potentials and have a greater probability of undergoing electron transfer reactions [2]. They form an important class of compounds due to their various properties and applications. Chalcones have attracted increasing attention due to numerous pharmacological applications such as antimalarial [3,4], anticancer [5,6], antiprotozoal (antileishmanial and antitrypanosomal) [7], anti-inflammatory [8,9], antibacterial [10], antifilarial [11], antifungal [12], antimicrobial [13], larvicidal [14], anticonvulsant [15], antioxidant [16] and antimitotic [17] activities. They have also shown inhibition of the enzymes, especially mammalian alpha-amylase [18], cyclo-oxygenase (COX) [19] and monoamine oxidase (MAO) [20]. Chalcones are also used for optical sensors [21], UV-absorption filters [22], ultrafast optical nonlinearities [23], and nonlinear optical (NLO) response [24] and as chemoprotective agent [25,26]. They are used as versatile starting materials for the synthesis of a variety of N, O containing heterocyclic compounds such as pyrazoline oxazoline and pyrimidine.

The description of the structure and energy of H-bonds continue to be a formidable task for both experimental and theoretical investigations. The infrared spectroscopy (IR), density functional theory (DFT), Atoms in molecules theory (AIM) [27] have becomes routine tools to analyze the H-bonding interactions in various systems. Among many leading factors, π electron delocalization is a very common effect influencing the characteristics of molecules and very often participating in chemical and biochemical process. The influence of π electron delocalization on intramolecular and intermolecular interaction was also noticed [27,28]. The influence of π electron delocalization on H-bonding interactions creates a special type of cooperatively called resonance resisted hydrogen bonding (RAHB). The electron density distribution governs all atomic and molecular properties. The quantum theory of atoms in molecules (QTAIM) has extensively been applied to classify and understand bonding interactions in terms of a quantum mechanical observable:

* Corresponding author. Tel.: +91 9451308205.
E-mail address: rnsvk.chemistry@gmail.com (R.N. Singh).

1386-1425/$ – see front matter © 2012 Elsevier B.V. All rights reserved.
http://dx.doi.org/10.1016/j.saa.2012.03.059

the electron density $\rho(r)$. The theory of AIM efficiently describes H-bonding and its concept without border. With respect to change of both the method used and the basis set the reliability and stability of values of AIM parameters have been studied and found that they were almost independent of basis set in case of used functional B3LYP in DFT [29]. One of the advantages of the AIM theory is that one can obtain information on changes in the electron density distribution as result of either bond formation or complexes formation.

As per literature the chalcone of ethyl 4-acetyl-3,5-dimethyl-1*H*-pyrrole-2-carboxylate with 2-chloro-benzaldehyde has not been reported. The interest in this compound provides opportunity for synthesis of new heterocyclic compounds which may have considerable pharmacological activities and material applications. It is interesting to mention that the pyrrole fragment is a constituent of many biological systems. Therefore, the title compound was synthesized and characterized. In the present paper we report the structure of ECPADMPC using quantum chemical calculations and experimental spectroscopic findings. Furthermore, quantum chemical calculations are also performed to find molecular structure, intra and intermolecular interactions and chemical reactivity of the title compound.

2. Experimental

2.1. Synthesis of ECPADMPC and spectral recording

The solvent methanol was dried and distilled before use according to the standard procedure [30]. Ethyl 4-acetyl-3,5-dimethyl-1*H*-pyrrole-2-carboxylate was prepared by an earlier reported method [31]. A ice cold mixture of ethyl 4-acetyl-3,5-dimethyl-1*H*-pyrrole-2-carboxylate (0.500 g, 2.38 mmol) and 2-chloro-benzaldehyde (0.3358 g, 2.38 mmol) in 50 ml ethanol was stirred for 30 min. A 5 ml of 40% aqueous sodium hydroxide solution was added dropwise. The reaction mixture was stirred at temperature 40–45° for overnight. The completion of the reaction was monitored by thin layer chromatography (TLC). Now the reaction mixture was neutralized with aqueous solution of HCl in an effort to aid product's precipitation and poured into crushed ice bath. After overnight, the creamy color precipitate was obtained. The precipitate was filtered off, washed with ethanol and dried in air. Yield 75.30%, m.p- 138–140 °C; The ^{1}H NMR and ^{13}C NMR spectra of EDPHEDPC were recorded in $CDCl_3$ on Bruker DRX-300 spectrometer using TMS as an internal reference. The UV–Vis absorption spectrum of EDPHEDPC (1×10^{-5} M in MeOH) was recorded on ELICO SL-164 spectrophotometer. The FT-IR spectrum was recorded in KBr medium on a Bruker spectrometer. The ESI-Mass spectrum was recorded on JEOL-Acc TDF JMS-T100L C mass spectrometer, MS (ESI): $m/z = 332$ (M+H), Elemental analyses were recorded on Elemental analyzer: VarioEL-III, Calculated C 65.29%, H 5.47%, N 4.22% and found C 65.38%, H 5.42%, N 4.20%.

3. Computational methods

In order to investigate the geometries, interaction energies and spectroscopic properties of the ECPADMPC, quantum-chemical calculations have been carried out. All quantum-chemical calculations have been performed using Gaussian 03 program package [32]. The molecular structure, FT-IR, ^{1}H NMR, ^{13}C NMR, UV–Vis and chemical reactivity were calculated using DFT, B3LYP functional and 6-31G(d,p) basis set. B3LYP invokes Becke's three parameter (local, non local, Hartree–Fock) hybrid exchange functional (B3) [33] with Lee–Yang–Parr correlation functional (LYP) [34]. The ^{1}H NMR and ^{13}C NMR chemical shifts and electronic absorption spectrum were calculated by employing Gauge Induced atomic orbital (GIAO) [35] and Time dependent density functional (TD-DFT) methods respectively. The ^{1}H NMR and ^{13}C NMR chemical shifts (δ_x) of any '*x*' proton or carbon are calculated by the difference between isotropic magnetic shielding (IMS) of TMS and respective '*x*' proton or carbon. It is defined by the equation: $\delta_x = IM_{TMS} - IMS_x$. The vibrational wavenumber calculation was also carried using B3LYP/6-31G(d,p) and scaled down using single scaling factor [36]. The frequency calculation produced positive wavenumbers indicating all stationary points as minima. Potential energy distribution along internal coordinates was calculated by Gar2ped software [37]. Internal coordinate system recommended by Pulay et al. was used for the assignment of vibrational modes [38]. All molecular geometries were visualized using Chemcraft [39] and Gauss-view [40] program. AIM calculation was performed by AIM2000 program [41].

4. Results and discussion

4.1. Thermodynamic properties and molecular geometry

The vibrational frequency calculations for all reactants and products were performed to determine the thermodynamic quantities at room temperature and their values are listed in Table 1. The optimized geometries of all the reactants and products involved in chemical reaction are shown graphically in Fig. 1, calculated at B3LYP/6-31G(d,p) level. For sake of simplicity both reactants ethyl 4-acetyl-3,5-dimethyl-1*H*-pyrrole-2-carboxylate and 2-chlorobenzaldehyde and product ECPADMPC and water are abbreviated as A, B, C and D respectively. For overall reaction the enthalpy change of reaction ($\Delta H_{Reaction}$), Gibbs free energy change of reaction ($\Delta G_{Reaction}$) and entropy change of reaction ($\Delta S_{Reaction}$) are found to be 5.89, 13.18 kcal/mol and −5.23 cal/mol K respectively. The reaction has positive values for $\Delta H_{Reaction}$, and $\Delta G_{Reaction}$ indicating that the reaction is endothermic and non-spontaneous at room temperature. This indicates that reaction will proceed at elevated temperature but the temperature gap will reduce in presence of catalyst and similar phenomenon was observed.

Optimized geometrical parameters of monomer (*syn*-conformer) calculated at B3LYP/6-31G(d,p) level are listed in Supplementary Table S1. Optimized geometry of the ground state *syn*- and *anti*-conformer with atomic numbering are shown in Fig. 2. They have energy −1437.42505127 and −1437.42476515 a.u. respectively, having the energy difference of 0.1795 kcal/mol at room temperature and existing in the ratio of 95.4:4.6 as per the Boltzmann distribution. The difference of dihedral angle τ(C3C2C6O7, 178.9051) between syn (179.2759°) and anti (−0.37082°) conformers brings carbonyl oxygen (O7) closer to hydrogen (H34) of β-methyl of pyrrole in anti conformer, and the consequences are repulsion between atom O7 and H34, increase of the angle C2C6O7 (126.53859°), decrease in surface area and volume and overall higher in energy. The volume of syn and anti conformers is 232.396 cm × 3/mol, 229.119 cm × 3/mol respectively. In case of the syn conformer the angle C2C6O7 (122.34716°) is less, whereas the surface area and volume are more than anti resulting to stabilization of the syn conformer. Therefore, all the calculations are carried out regarding most stable *syn*-conformer. The asymmetry in pyrrole ring is reflected through bond difference of the N1—C2 and N1—C5 and can be explained by electron withdrawing character of the ethoxycarbonyl group. The asymmetry in pyrrole ring is not only evident in this quantum chemical calculation but also reflected in the crystal structures of the ethyl-3,5-dimethyl-1*H*-pyrrole-2-carboxylate [42] and methyl 4-p-tolyl-1*H*-pyrrole-2-carboxylate [43]. In equilibrium geometries of dimer chloro benzene plane is twisted from alkene plane with significant dihedral angle (C18C16C15C14 −21.16°).

Table 1
Calculated enthalpy (a.u.), Gibbs free energy (a.u.), entropy (cal/mol K) for A, B, C, D and reaction.

Thermodynamic parameters	A	B	C	D	Reaction
Enthalpy (*H*)	−708.42	−805.06	−1437.1	−76.40	0.01
Gibbs free energy (*G*)	−708.48	−805.11	−1437.2	−76.42	0.02
Entropy (*S*)	129.89	86.61	166.15	45.12	−5.23

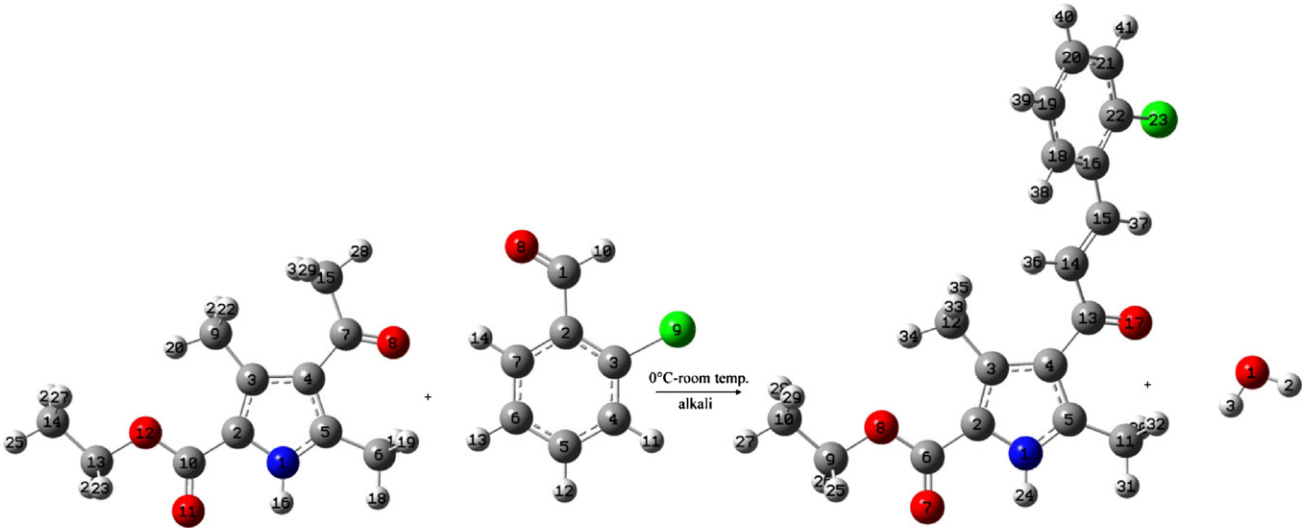

Fig. 1. The optimized geometries of the reactants and products involved in chemical reaction.

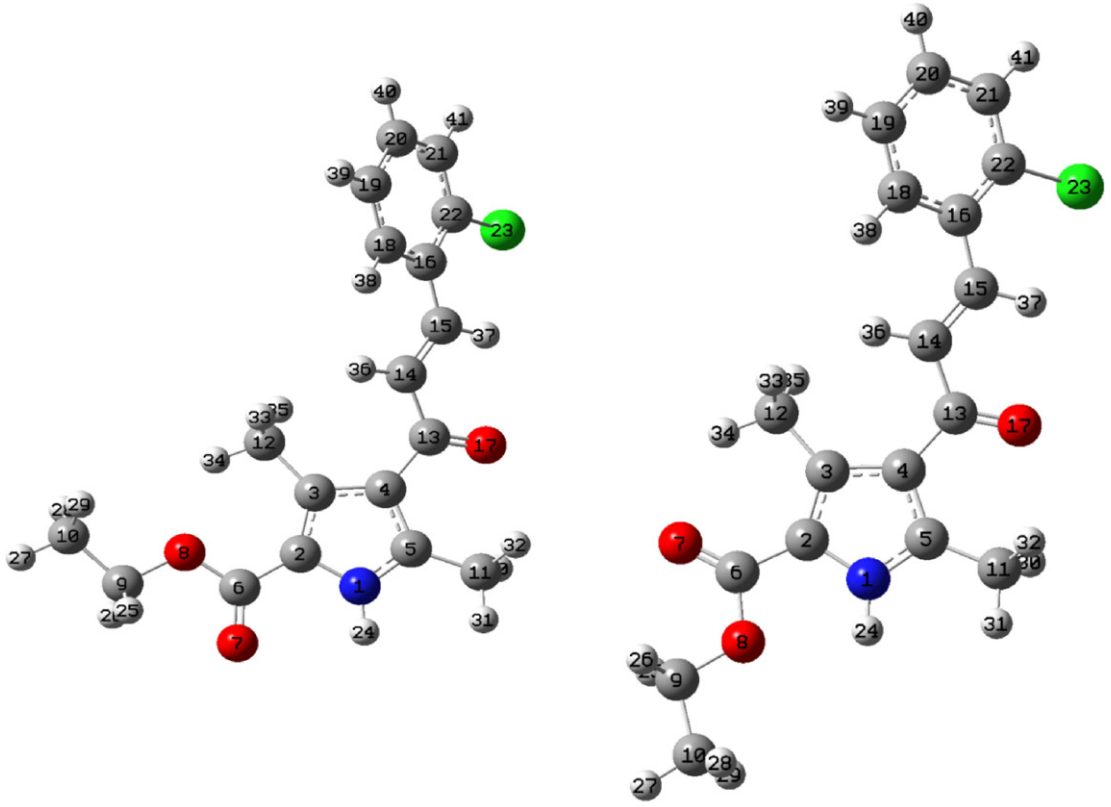

Fig. 2. The optimized geometries of ground state (*syn*)- and (*anti*)-conformer of ECPADMPC at B3LYP/6-31G(d,p) level.

Table 2
The Thermodynamics quantities (enthalpy, Gibbs free energy, entropy), their change and equilibrium constant of conversion from monomer to dimer.

Parameters	Enthalpy (H) (a.u.)	Gibbs free energy (G) (a.u.)	Entropy (S) (cal/mol K)	ΔH (kcal/mol)	ΔG (kcal/mol)	ΔS (cal/mol K)	K_{eq}
2 × monomer	−2874.15	−2874.32	332.30	−12.45	−1.38	−37.12	10.35
Dimer	−2874.17	−2874.31	295.18				

The explanation for the twisting or deviation of one plane from another is repulsion between the proximal hydrogen and chlorine. The experimental and computational data show that H-bonding exerts substantial changes on the molecular geometry of the distant parts of the system. These changes are related to the variations in π-electron delocalization and reflect the strength of H-bonding. The optimized geometry of dimer for the most stable *syn*-conformer with atomic numbering is shown in Fig. 3. In dimer, intermolecular dihydrogen bonds formed between pyrrolic (N1—H24) and carbonyl (C6=O7) oxygen of ester. In dimer both molecules exist in *s-cis* form, with N1—H24 bond as proton donor and C6=O7 bond as proton acceptor. According to the Etter terminology [44], the cyclic ester dimer forms the ten membered ring denoted as $R_2^2(10)$ or more extended sixteen membered ring $R_2^2(16)$. The superscript designates the number of acceptor centers and the subscript, the number of donors in the motif. In dimer, due to intermolecular hydrogen bond formation both proton donor (N—H bond) and proton acceptor (C=O bond) are elongated by 0.00990 Å and 0.00847 Å respectively. The binding energy of the analyzed dimer is computed as the difference between the calculated total energy of the dimer and the energies of the two isolated monomers. The total energy and binding energy of dimer are calculated as −2874.87 a.u., −13.92 kcal/mol respectively using DFT calculations. The binding energy of dimer is computed as the difference between the calculated total energy of the dimer and the energies of the two isolated monomers and found to be −13.92 kcal/mol. The calculated hydrogen binding energy of dimer formation has been corrected for the basis set superposition error (BSSE) via the standard counterpoise method [45] and found to be −9.72 kcal/mol. The calculated changes in thermodynamic quantities during the dimer formation in gaseous phase have the negative values of ΔH (kcal/mol), ΔG (kcal/mol) and ΔS (cal/mol K) indicating that the dimer formation is exothermic and spontaneous. The calculated equilibrium constant between monomer and dimer is quite high ($K = 10.35$) indicating that dimer formation is highly preferred and as a result even anti conformer gets converted to syn and finally forms the dimer. The Thermodynamics quantities (enthalpy, Gibbs free energy, entropy), their change and equilibrium constant of conversion from monomer to dimer are given in Table 2.

4.2. ^1H NMR and ^{13}C NMR spectroscopy

The ^{1}H NMR and ^{13}C NMR chemical shifts of ECPADMPC were calculated with GIAO approach at B3LYP/6-31G(d,p) level [35]. The experimental ^{1}H NMR spectrum is shown in Fig. 4. The experimental and calculated ^{1}H NMR chemical shifts of ECPADMPC are listed in Supplementary Table S2. The correlation between the experimental and calculated chemical shifts are compared and found to follow the linear equation ($Y = mX + C$) where Y is the experimental ^{1}H NMR chemical shifts (δ in ppm), m is the slope having value 0.99666, X is the calculated ^{1}H NMR chemical shifts (δ in ppm) and C is the constant having value 3.1924. The value of correlation coefficient ($R^2 = 0.99$) shows that there is a good agreement between experimental and calculated ^{1}H NMR chemical shifts. The ^{1}H NMR correlation graph is shown in Fig. 5. The experimental and calculated ^{13}C NMR chemical shifts of ECPADMPC are listed in Supplementary TS3. The ^{13}C NMR correlation graph is shown in Fig. 6. The value of correlation coefficient ($R^2 = 0.99$) for ^{13}C NMR indicates that there is a good agreement between experimental and calculated results.

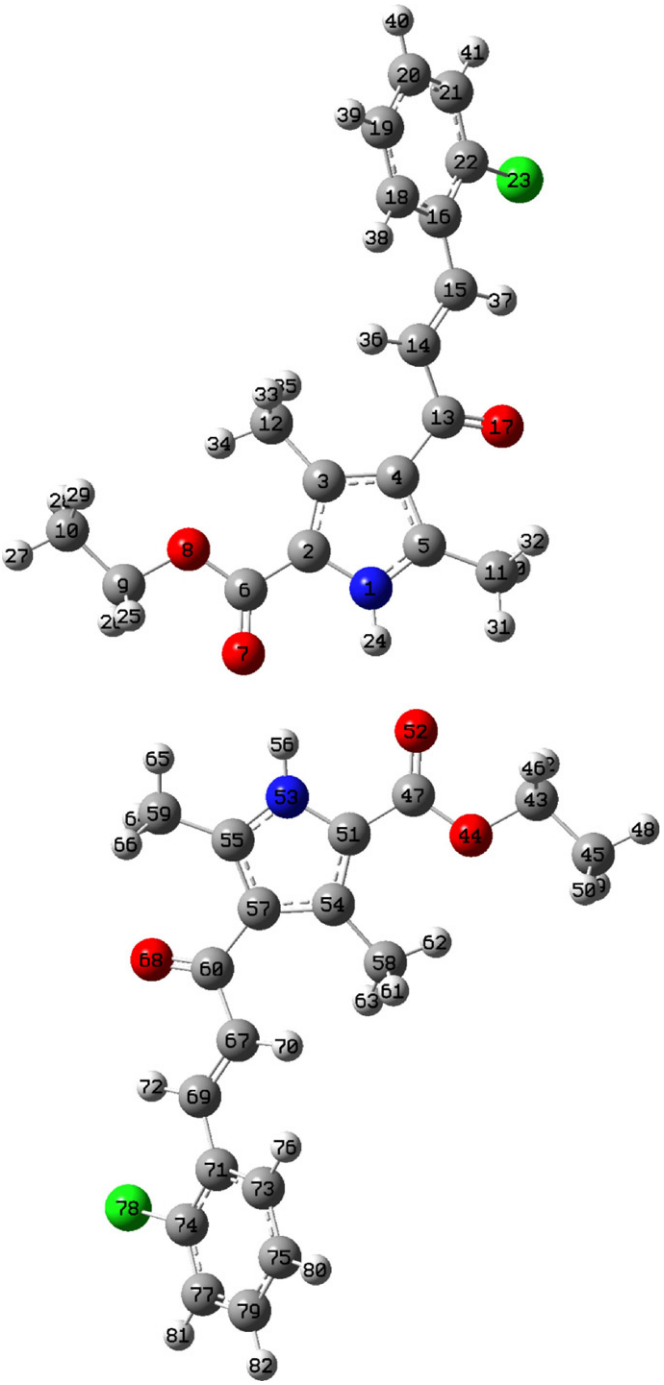

Fig. 3. The optimized geometry of dimer for (*syn*)-conformer at B3LYP/6-31G(d,p) level.

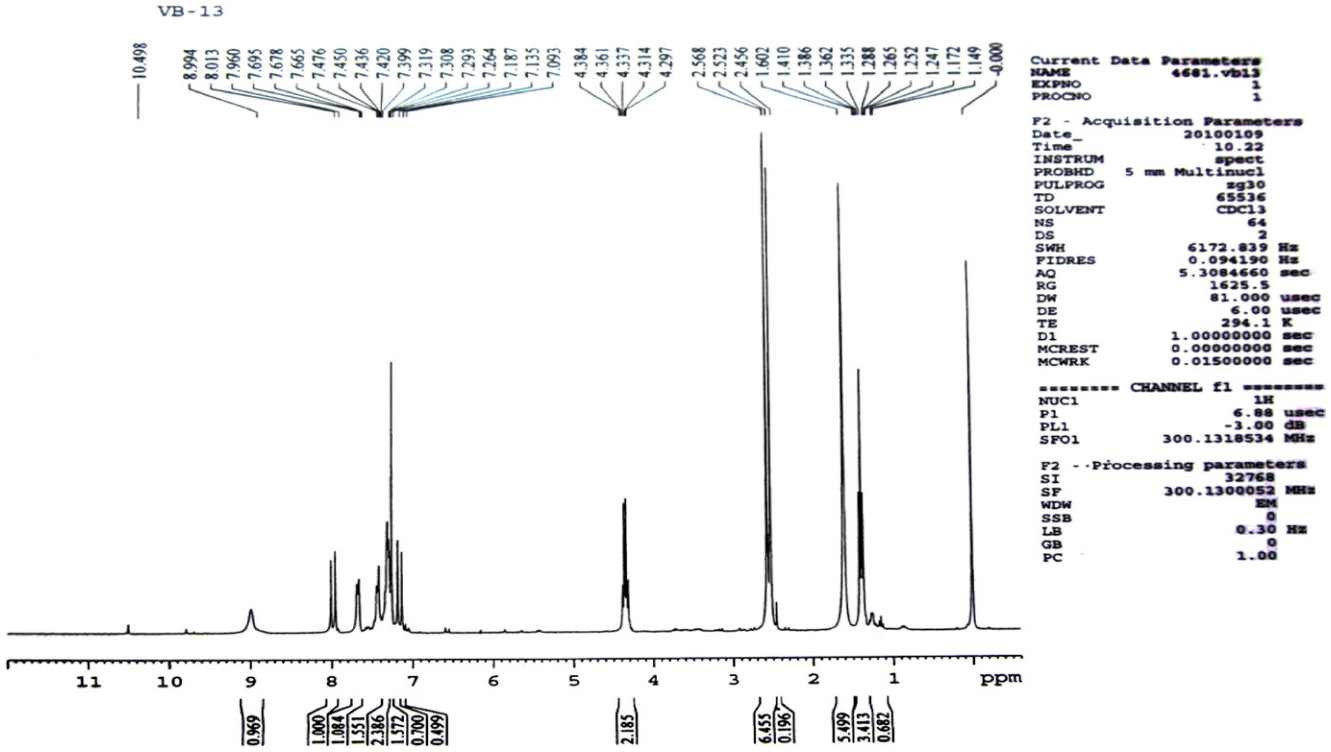

Fig. 4. Experimental ^{1}H NMR spectrum of ECPADMPC.

4.3. UV–visible spectroscopy

To obtain the nature of the transitions, electronic excitation energies and oscillatory strength the UV–visible spectrum of ECPADMPC has been studied by the time-dependent density functional theory (TD-DFT). The observed and calculated electronic transitions of high oscillatory strength are given in Table 3. Experimental UV–Vis spectrum is shown in Fig. 7. The molecular orbitals are shown in Fig. 8. The HOMO-LUMO energy gap is an important stability index which reflects the chemical stability of the molecule. The HOMO–LUMO energy gap of ECPADMPC calculated at B3LYP/6-31G(d,p) level is.

HOMO energy = −6.0007 eV
LUMO energy = −1.9739 eV
HOMO–LUMO energy gap = 4.0268 eV.

The three intense calculated electronic transitions at λ_{max} = 303.74 nm, f = 0.5101; λ_{max} = 281.87 nm, f = 0.1744 and λ_{max} = 251.31 nm, f = 0.1705 have been obtained which corresponds to the experimental λ_{max} values at 346, 270 and 228 nm, respectively. The molecular orbital coefficients analyses confirm that these electronic excitations are $\pi \rightarrow \pi^*$ and $n \rightarrow \pi^*$ in nature. The observed λ_{max} at 346 nm shows red shift compared with the experimental data. The observed λ_{max} at 270 and 228 nm show blue shift compared with the experimental data. The longest

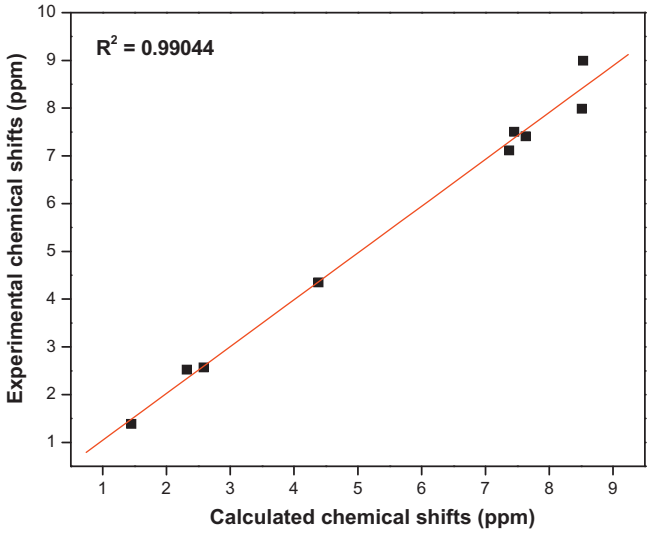

Fig. 5. The correlation graph between experimental and calculated ^{1}H NMR chemical shifts.

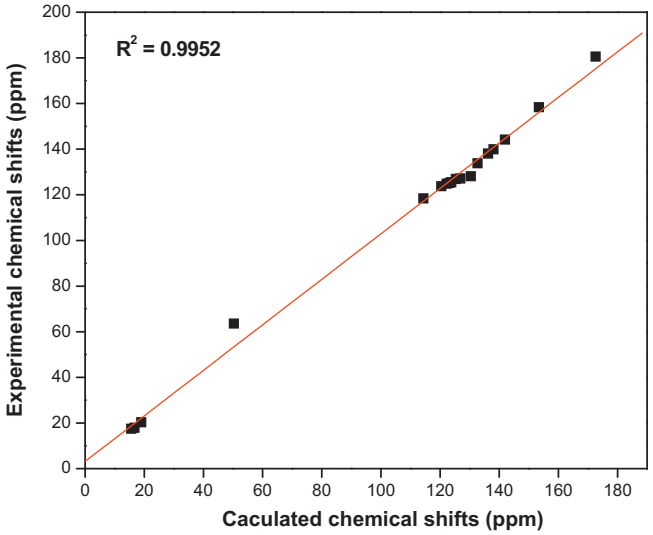

Fig. 6. The correlation graph between experimental and calculated ^{13}C NMR chemical shifts.

Table 3
Comparison between experimental and calculated electronic transitions: *E*/eV, oscillatory strength (*f*), (λ_{max}/nm) at TD-DFT/B3LYP/6-31G(d,p) level.

S. no.	Electronic transitions	*E* (eV)	Oscillatory strength (*f*)	Calculated (λ_{max})	Observed (λ_{max})	% contribution of probable transition	Assignment
1	H−4→L	4.082	0.5101	303.74	346	3.39	$\pi \rightarrow \pi^*$
	H−3→L					6.36	
	H−2→L					15.86	
	H−1→L					17.53	
2	H−4→L	4.3986	0.1744	281.87	270	23.38	$\pi \rightarrow \pi^*$
	H−3→L					10.48	
	H−2→L					1.216	
	H−1→L					5.48	
	H−1→L+2					1.84	
	H→L+1					1.07	
3	H−5→L	4.9335	0.1705	251.31	228	1.911	$n \rightarrow \pi^*$
	H−5→L+1					1.981	
	H−2→L+1					7.18	
	H−1→L+1					10.64	
	H→L+1					21.57	

wavelength band at 346 nm originates due to the combination of 'H−2→L and H−1→L' transitions with 15% and 17% contribution respectively, similarly the observed band at 270 and 228 nm originate due to the H−4→L and H→L+1 transition respectively.

4.4. Vibrational assignments

Calculated and experimental IR-spectrum of ECPADMPC in the region 400–4000 cm^{-1} is shown in Fig. 9. Theoretical (calculated and scaled) and experimental vibrational wavenumbers (in cm^{-1}) with their assignment are given in Table 4. The total number of atoms in monomer and dimer are 41 and 82 respectively. Therefore, they give 117 and 240, (3*n*−6) vibrational modes for monomer and dimer respectively. The calculated vibrational wavenumbers are higher than the experimental wavenumbers due to discard of anharmonicity present in real system. Therefore, calculated wavenumbers are scaled down by a single factor 0.9608 [36] to compare with experimental wavenumbers. The value of correlation coefficient (R^2 = 0.99) shows that there is a good agreement between experimental and calculated wavenumbers. The correlation graph is shown in Fig. 10. The scaled vibrational wavenumbers with their potential energy distribution (PED) help in the assignment of vibrational modes obtained from experimental FT-IR spectrum. Gauss-view program is also used to assign the calculated harmonic vibrational wavenumbers. The wavenumbers are differ in greater extent for pyrrole (N—H) and ester carbonyl (C=O) in monomer and dimer. The experimental wavenumbers are in close agreement with the calculated wavenumbers of dimer than monomer. Therefore, assignment is performed using dimer PED. The calculated vibrational wavenumbers of monomer with their assignment are given in Supplementary Table S4. The monomers as well as the dimer possess C1 symmetry; therefore the vibrational modes will be active for both IR and Raman. The Raman spectrum of the dimer was calculated and found equal in frequencies and intensities.

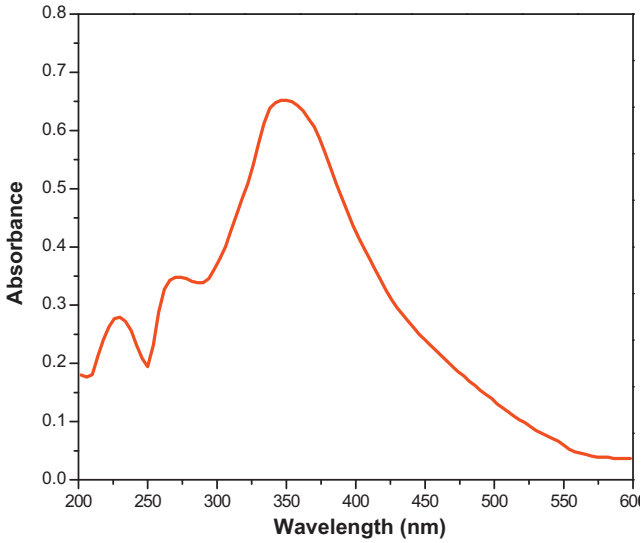

Fig. 7. Experimental UV–Vis spectrum of ECPADMPC.

4.4.1. N—H vibrations

The FT-IR spectrum of ECPADMPC is studied in the solid state at room temperature. In the Dimer formation elongation of N—H bond and red shift is observed as compared to monomer [46]. The bands ascribed to stretching and out-of-plane deformation vibrations of NH group involved in NH···O hydrogen bonds was analyzed. The N—H stretch of pyrrole (ν_{N-H}) is observed at 3266 cm^{-1}, whereas this is calculated as 3333 cm^{-1} in dimer and 3497 cm^{-1} in monomer. The observed wavenumber at 3266 cm^{-1} is in good agreement with the calculated wavenumber of dimer. The observed value of ν_{N-H} also correlates with the earlier reported intermolecular hydrogen bonded N—H absorption band at 3358 cm^{-1}, recorded in KBr pellet for pyrrole-2-carboxylic acid [46]. In solid state spectrum of ECPADMPC attributes to the vibration of hydrogen bonded N—H group and the observed wagging mode at 756 cm^{-1}, whereas this is calculated as 759 cm^{-1} in dimer and absent in monomer confirms the involvement of pyrrole N—H group in intermolecular attraction. The frequencies appearing due to N—H···O stretching, bending, and torsional modes' contribute to certain modes but the main contributions are to C=O and N—H frequencies and that also to less than 3%. The PED assignment has been considered and incorporated for contributors more than 5%, therefore N—H···O stretching, bending, and torsional modes' contributions are not appearing in IR Table 4.

4.4.2. C—H vibrations

As decreases in C—H bond lengths and blue shifts of the corresponding stretching vibration frequencies are contrary to the features of conventional H-bonds, interactions exhibiting such characteristics have been classified as anti-H-bonds [47]. The blue shift is clearly observed by comparing the result of monomer and Dimer. From an electron density topology analysis it has been concluded that the anti-H-bond or conventional H-bonds pattern originates from the specific redistribution of electron density in

Table 4
Experimental and calculated (selected) vibrational wavenumbers of dimer and their assignments: Wavenumbers ($\bar{V}$/cm^{-1}), (IR_{int}/kmmol^{-1}).

Mode no.	$\bar{V}$ calculated		IR_{int}	$\bar{V}$ obs	Assignment (PED ≥ 5%)
	Unscaled	Scaled			
240	3469	3333	2862.49	3266	ν(N1—H24)(50)–ν(N53—H56)(47)
239	3463	3327	9.54		ν(N1—H24)(49) ν(N53—H56)(47)
238	3225	3099	7.14		ν(C67—H70)(78) ν(C14—H36)(14)
237	3225	3099	16.23		ν(C14—H36)(78)–ν(C67—H70)(14)
235	3222	3096	12.45		(ν(C77—H81)(65) ν(C79—H82)(14)–ν(C21—H41)(11)
234	3212	3086	11.84	3065	ν(C19—H39)(41) ν(C18—H38)(36)–ν(C21—H41)(13) ν(C20—H40)(6)
233	3212	3086	10.4		ν(C75—H80)(41) ν(C73—H76)(36)–(ν(C77—H81)(13) ν(C79—H82)(6)
230	3201	3076	5.49		ν(C20—H40)(39)–ν(C18—H38)(36) ν(C15—H37)(7)–ν(C21—H41)(6)
229	3201	3076	14.77		ν(C79—H82)(39)–ν(C73—H76)(36) ν(C69—H72)(7)–(ν(C77—H81)(6)
226	3171	3047	11.76		ν(C58—H62)(45)–ν(C12—H34)(40)–ν(C58—H63)(7) ν(C12—H35)(6)
224	3153	3029	7.74		ν(C11—H31)(47)–ν(C11—H32)(21)–τ(C11—C5)(18)–ν(C11—H30)(5)
223	3153	3029	12		τ(C59—C55)(27)–ν(C59—H65)(25)–(δ′ asym-Me6)(16) ν(C59—H66)(11) τ(C59—C10)(11)
222	3141	3018	59.54	2983	τ(C10—C9)(41)τ(C59—C10)(21) ν(C45—H50)(7) ν(C10—H29)(6)–ν(C45—H49)(6) ν(C10—H28)(5)
221	3141	3018	2.46		τ(C10—C9)(44)τ(C59—C10)(23) ν(C10—H29)(6)–ν(C45—H50)(5)–ν(C10—H28)(5)
220	3133	3010	44.99		ν(C45—H48)(33)–ν(C10—H27)(25)–ν(C45—H49)(11) ν(C10—H28)(9)–ν(C45—H50)(7) ν(C10—H29)(5)
218	3125	3003	7.68		(ω-C59C55)(19)τ(C59—C10)(17)–τ(C59—C55)(11) ν(C59—H64)(10)–ν(C59—H66)(8)–(δ′ asym-Me6)(6)–(ρ-Me6)(6) (ω-C11C5)(5)
216	3111	2989	23.75		ν(C12—H35)(41) ν(C58—H63)(32)–ν(C12—H33)(9)–ν(C58—H61)(7) ν(C12—H34)(5)
215	3111	2989	6.77		ν(C58—H63)(41)–ν(C12—H35)(32)–ν(C58—H61)(9) ν(C12—H33)(7) ν(C58—H62)(5)
214	3108	2986	11.1		(ρ-CH_2)(24)–ν(H42—C43)(23) (δ-C47C43O44)(14)–τ(C47—C51)(9) ν(C43—H46)(9)
212	3066	2946	52.1		ν(H42—C43)(44)–(δ-C47C43O44)(26)–ν(C9—H26)(10) ν(C43—H46)(9)–ν(C9—H25)(8)
209	3062	2942	19.09		ν(C11—H30)(21)ν(C11—H31)(17) ν(C11—H32)(15)–ν(C59—H64)(11)–ν(C59—H65)(9)–ν(C59—H66)(8)-τ(C59—C10)(7)
207	3057	2937	31.73	2928	ν(C10—H27)(19)ν(C10—H28)(18) ν(C10—H29)(17)–ν(C45—H48)(16)–ν(C45—H49)(15)–ν(C45—H50)(14)
205	3036	2917	63.99		ν(C58—H61)(43)–ν(C12—H33)(40) ν(C58—H63)(6)–ν(C12—H35)(6)
204	1731	1663	475.01	1669	(δ-C47C43O44)(29)–(ρ-C51C47)(10)–(δ-C47O52C51)(8) ν(C47—O52)(5)–(δ-C47C51)(5)–ν(C6—O7)(5)
203	1728	1660	7.01		(δ-C47C43O44)(16)(δ′ asym-Me6)(15)–τ(C59—C10)(6)–(ρ-C51C47)(6) ν(C60—O68)(6) ν(C13—O17)(6)
202	1718	1651	24.33		(δ-C47C43O44)(36)–(ρ-C51C47)(13)–(δ-C47O52C51)(8) ν(C47—O52)(7) ν(C6—O7)(6)–(δ-C47C51)(5)
201	1717	1650	1963.81	1591	(δ-C47C43O44)(28)–(ρ-C51C47)(9) τ(C11—C43)((8)–(δ-C47O52C51)(7)–(δ′ asym-Me6)(6) τ(C59—C9)(6) ν(C47—O52)(5)–ν(C6—O7)(5)
199	1657	1592	406.64		(δ′ asym-Me6)(16)ν(C67—C69)(11)–ν(C14—C15)(11)–τ(C59—C10)(9) ν(C60—O68)(9)–ν(C13—O17)(9)
198	1646	1581	9.61		ν(C73—C75)(13)ν(C18—C19)(11) ν(C74—C77)(8) ν(C21—C22)(7) (δ asym-R4)(5)
197	1646	1581	67.11		ν(C18—C19)(12)–ν(C73—C75)(11) ν(C21—C22)(8)–ν(C74—C77)(7) (δ asym-R2)(5)
195	1615	1552	17.26		ν(C75—C79)(15)–ν(C19-20)(14)–ν(C77—C79)(8) ν(C20—C21)(7)–(δ-H82C79)(6) (δ-H40C20)(6) ν(C71—C74)(6)–ν(C16—C22)(5)–ν(C71—C73)(5.) ν(C16—C18)(5.)
194	1606	1543	10.09		τ(C11—C43)(16)(δ′ asym-Me6)(13)–(δ-N1H24)(7)–τ(C59—C9)(7) ν(C53—C55)(5)
193	1598	1535	341.53		(δ′ asym-Me6)(19)(δ-N1H24)(8) +)–τ(C59—C55)(6) τ(C11—C43)(5)–(ω-H56N53)(5)
192	1562	1501	367.39		τ(C59—C10)(26)–(δ′ asym-Me6)(21) τ(C11—C43)(18) τ(C59—C9)(13)
191	1560	1499	7.89	1480	τ(C59—C10)(35)–(δ′ asym-Me3)(32) τ(C59—C55)(6) (δ asym–Me6)(5)
189	1533	1473	6.06		τ(C11—C43)(36)–(δ sc-CH_2)(34) (δ sc-CH_2)(8) τ(C59—C9)(7)
187	1522	1462	231.71		τ(C59—C10)(40)–(δ′ asym-Me6)(23) τ(C59—C55)(9) τ(C59—C9)(7) (δ asym–Me6)(7) τ(C11—C43)(6)
184	1510	1451	76.25		τ(C59—C10)(42)–(δ′ asym-Me6)(23) τ(C59—C55)(8) (δ sc-CH_2)(6)
183	1510	1451	20.19		(δ′ asym-Me6)(31)–τ(C59—C10)(17)–τ(C59—C55)(11) τ(C11—C43)(7)–τ(C59—C9)(6)–(δ asym-Me6)(6)
182	1509	1450	32.26		τ(C59—C10)(51)-(δ′ asym-Me6)(16) τ(C59—C55)(6) (δ sc-CH_2)(6) τ(C10—C9)(5)
179	1501	1442	13.59		τ(C10—C9)(50)τ(C59—C10)(49)
177	1498	1439	26.42		τ(C10—C9)(41)(δ′ asym-Me6)(18) τ(C59—C10)(15)
176	1489	1431	26.4	1430	(δ′ asym-Me3)(57)(δ sym-Me6)(24) (ρ-Me3)(6)
175	1489	1431	5.85		(δ′ asym-Me6)(60)(δ asym-Me6)(24)
173	1481	1423	344.93		(δ asym-Me6)(36)τ(C59—C55)(33)–τ(C11—C5)(12)

Table 4 (*Continued*)

Mode no.	$\tilde{V}$ calculated		IR_{int}	$\tilde{V}$ obs	Assignment (PED ≥ 5%)
	Unscaled	Scaled			
172	1478	1420	32.49		τ(C59—C55)(30)(δ asym-Me6)(22)–(δ′ asym-Me6)(13) τ(C11—C5)(10) τ(C59—C10)(8)
171	1478	1420	48.84		τ(C59—C55)(31)(δ asym–Me6)(24)–τ(C11—C5)(11)–(δ′ asym-Me6)(9) τ(C59—C10)(5)
170	1467	1409	8.84		τ(C59—C10)(33)–(δ′ asym-Me6)(29)–τ(C11—C43)(11) τ(C59—C9)(9) τ(C59—C55)(8)
169	1466	1409	441.4		τ(C59—C10)(45)–(δ′ asym-Me6)(32) τ(C59—C55)(9)–τ(C11—C5)(3) τ(C59—C9)(3)
167	1438	1382	27.43	1378	τ(C11—C43)(28) (δ sym-Me3)(32) (ω-CH_2)(6)–(ω-CH_2)(6)-(δ sym-Me6)(5)
163	1428	1372	78.82	1352	τ(C59—C10)(59)–(δ sym-Me6)(11) (δ sym-Me3)(10) τ(C11—C43)(9) τ(C59—C9)(9)
161	1401	1346	17.36		(ω-CH_2)(26)–(ω-CH_2)(26)–τ(C11—C43)(19)–τ(C59—C9)(8) τ(C59—C10)(6)
159	1391	1336	186.22	1305	τ(C11—C43)(27) τ(C59—C9)(16) (ω-CH_2)(15)–(ω-CH_2)(14)–(δ′ asym-Me6)(8) τ(C59—C10)(7) τ(C59—C55)(6)
157	1354	1301	145.09		(ω-CH_2)(22)–(ω-CH_2)(21) τ(C11—C43)(20) τ(C59—C9)(11)
156	1346	1293	36.3		(ω- CH_2)(20)–(ω-CH_2)(19) τ(C11—C43)(15) τ(C59—C9)(9)–τ(C59—C10)(7) (δ′ asym-Me6)(5)
154	1320	1268	22.2		τ(C11—C43)(22)–τ(C59—C9)(17)–(ω-CH_2)(15)-(ω-CH_2)(14) (δ′ asym-Me6)(10)–τ(C59—C55)(7)
153	1317	1265	979.3		τ(C11—C43)(19)(ω-CH_2)(18)–(ω-CH_2)(17) τ(C59—C9)(14) (δ′ asym-Me6)(10)–τ(C59—C55)(7)
151	1310	1259	21.31		(δ-H38C18)(12)–(δ-H76C73)(12) (δ-H41C21)(6)–(δ-H81C77)(6)–ν(C15—C16)(5) ν(C69—C71)(5)–τ(C11—C43)(5)
149	1309	1258	161.44	1280	τ(C11—C43)(28)τ(C59—C9)(13) (ω-CH_2)(11)–(ω-CH_2)(10) (δ′ asym-Me6)(7)–(δ sym–Me6)(5) (δ sym-Me3)(5)
145	1260	1211	56.07	1196	τ(C11—C43)(17) τ(C59—C10)(12) τ(C59—C9)(11) τ(C59—C55)(10) (ω-CH_2)(6)–(δ′ asym-Me6)(6)–(ω-CH_2)(6)
143	1233	1185	18.07		(δ-H41C21)(8)–(ρ–H37C15)(8) ν(C15—C16)(7)–(δ-H81C77)(6)–ν(C18—C19)(6) (ρ-H72C69)(6)–ν(C69—C71) (6)–(δ-H39C19)(6) ν(C73—C75)(5.)
142	1218	1170	10.07		τ(C11—C43)(25)–(ω-CH_2)(15)–(ω-CH_2)(15)–τ(C59—C9)(14)–(δ-C47O52C51)(7)–τ(C59—C55)(5)
141	1217	1169	645.52		(ω-CH_2)(19)–(ω-CH_2)(18) τ(C59—C9)(11)–(δ-C47O52C51)(9)–τ(C59—C10)(8) τ(C11—C43)(7)
138	1185	1139	7.54		τ(C59—C10)(30)–(ρ–CH_2)(21)–τ(C11—C43)(19) τ(C10—C9)(9)–τ(C59—C9)(8)
136	1150	1105	7.83		ν(C77—C79)(8)ν(C20—C21)(8)–(δ-H82C79)(8)–(δ-H40C20)(7) ν(C74—C77)(6) ν(C21—C22)(6) (δ-H76C73)(5) (δ-H38C18)(5)
135	1150	1105	8.74		ν(C20—C21)(8)–ν(C77—C79)(8)–(δ-H40C20)(8) (δ-H82C79)(7) ν(C21—C22)(6)–ν(C74—C77)(6) (δ-H38C18)(5)–(δ-H76C73)(5)
133	1142	1097	34.92	1096	(ρ-Me1)(55)–τ(C59—C10)(19)–(δ-C47C43O44)(11) (δ sc-C9H25H26)(5)
132	1128	1084	5.59		(ρ-Me1)(41)–τ(C59—C10)(19)–(δ-C47O52C51)(5)
131	1127	1083	201.76	1063	(ρ-Me1)(34)–τ(C59—C10)(16) (δ-C47O52C51)(5)
129	1078	1036	112.54		τ(C59—C55)(22)(ρ-Me3)(18)–(δ′ asym-Me6)(15)–(ρ-Me6)(13)–τ(C11—C5)(8)
128	1075	1033	12.54		(ρ-Me3)(21)–(ρ-Me6)(15) τ(C59—C55)(14)–(δ′ asym-Me6)(14) τ(C59—C10)(7) (ω-C59C55)(5)–τ(C11—C5)(5)
126	1067	1025	6.75		τ(C59—C10)(36)(ω-C59C55)(11)–(ρ-Me3)(10) (ω-C11C5)(8)–(ρ-Me6)(7)–τ(C59—C55)(7) τ(C59—C9)(7) τ(C11—C43)(7)
122	1054	1013	62.3		(δ tri-R2)(20)(δ tri-R4)(20)–ν(C22—Cl23)(7)–ν(C74—Cl78)(7)
121	1054	1013	37.63		(δ tri-R4)(21)–(δ tri-R2)(20)–ν(C74—Cl78)(7) ν(C22—Cl23)(7)
119	1049	1008	74.67	1006	τ(C11—C43)(34)–τ(C59—C10)(16) (ρ-Me3)(8) (δ-C47C43O44)(6) τ(C59—C9)(5)-(ρ-Me1)(5)
118	1031	990.6	25.18		τ(C14—C15)(32)(ω-H37C15)(26) τ(C59—C55)(7)–(ω-C13C14)(6) τ(C67—C69)(5)
117	1031	990.6	26.19		τ(C67—C69)(36)(ω-H72C69)(30)–(ω-C60C67)(7)–τ(C14—C15)(5)
116	1029	988.7	305.89	977	τ(C59—C55)(42)–τ(C11—C5)(15)–(δ′ asym-Me6)(13) (ρ-Me3)(12)–(ρ-Me6)(9)
114	1014	974.3	154.96		τ(C59—C55)(38)–(δ′ asym-Me6)(17)–τ(C11—C5)(14) (ρ-Me3)(12)–(ρ-Me6)(8)
108	918.7	883.7	5.23	883	τ(C11—C43)(18)τ(C59—C10)(17)–(ρ-Me1)(13)–(ω-CH_2)(9)–(ω-CH_2)(9)–τ(C59—C9)(6)
107	917.6	881.6	13.36		τ(C11—C43)(15)(ρ-Me1)(12)–τ(C59—C10)(10) τ(C59—C9)(10) (ω-CH_2)(9)–(ω-CH2)(9)–τ(C59—C55)(6)
105	903.6	868.2	17.78		τ(C59—C9)(19)τ(C11—C43)(18) (ρ-Me1)(18) (ω-CH_2)(12)–(ω-CH_2)(12)–τ(C59—C10)(9) (δ-C47C43O44)(5)
103	891.9	856.9	5.78		τ(C59—C9)(19)–(ω-C59C55)(12) (ρ-Me1)(8)–(ω-C11C5)(8)–(δ-C47C43O44)(7)–(τ′-R1)(5) (ω-CH_2)(5) (ω-CH_2)(5)
98	838.5	805.6	108.28		(ω-N1H24)(49)τ(C59—C9)(45)

Table 4 (*Continued*)

Mode no.	$\tilde{V}$ calculated		IR_{int}	$\tilde{V}$ obs	Assignment (PED ≥ 5%)
	Unscaled	Scaled			
94	803.5	772	26.79		τ(C59—C9)(13)(δ-C47C43O44)(13)τ(C59—C10)(9)–(ω-C59C55)(7) (τ′-R1)(5) (ω-C11C5)(5)
93	790.4	759.4	5.99	756	τ(C59—C9)(42)(ω-N1H24)(40)
92	780.7	750.1	24.33		(ω-C59C55)(25)-(ω-C11C5)(18)–τ(C59—C10)(6)–τ(C59—C55)(6)–(τ′-R1)(6) (ω-C47C51)(6) (ω-N1H24)(5)–(ω-C6C2)(5)
91	779.1	748.6	30.94		(ω-C59C55)(30)(ω-C11C5)(22)–τ(C59—C55)(9) (τ′-R1)(8)–τ(C59—C10)(8) (τ′-R3)(5)
90	769.1	739	52.13		(ω-C59C55)(15)–(ω-C11C5)(11)–(τ′-R1)(10)–τ(C59—C55)(9)–τ(C59—C10)(9)–(δ-C47C43O44)(8) (δ-C47O52C51) (7) (τ′-R3)(6)
89	763.8	733.9	9.26		(ω-C59C55)(28)(ω-C11C5)(21)–τ(C59—C10)(8)–τ(C59—C55)(7) (ω-C47C51)(6) (τ′-R1)(6) (ω-C6C2)(5)
88	761.1	731.3	6.68		(ω-C59C55)(29)–(ω-C11C5)(21)–τ(C59—C55)(10)–τ(C59—C10)(8)–(τ′-R1)(7)
86	751.5	722	11.59	683	(ω-C47C51)(34)(ω-C6C2)(28)–(τ′-R1)(12)–(τ′-R3)(7) τ(O8—C6)(7) τ(C47—C51)(5)
82	695.3	668	19.73		(ω-C59C55)(31)(ω-C11C5)(22)–τ(C59—C55)(10) (ω-C47C51)(5)
81	695.3	668	20.71		(ω-C59C55)(28)–(ω-C11C5)(20)–τ(C59—C55)(9) (ω-C47C51)(6)–τ(C59—C10)(6) –(ω-C6C2)(5)
80	674.5	648.1	28.15		(ω-C59C55)(31)–(ω-C11C5)(23)–(τ′-R1)(14)–τ(C59—C55)(9) (τ′-R3)(9)
79	673.4	647	0.78	629	(ω-C59C55)(31)(ω-C11C5)(22) (τ′-R1)(13)–τ(C59—C55)(9) (τ′-R3)(8)–τ(C59—C10)(5)
78	646.9	621.5	30.75		(ω-C47C51)(34)–(ω-C6C2)(24) (τ′-R1)(13)–(τ′-R3)(10)
77	646.9	621.5	5.45		(ω-C47C51)(29)(ω-C6C2)(28)–(τ′-R1)(21)–(τ′-R3)(11)
73	600.5	577	59.21	577	τ(C59—C10)(30)–(ω-C59C55)(21) (ω-C11C5)(16) (τ′-R1)(6)
71	581.6	558.8	33.68		τ(C59—C10)(33)–(ω-C59C55)(19) (ω-C11C5)(14) (τ′-R1)(9)–(τ′-R3)(5)
70	534.9	513.9	14.67	448	(ω-C59C55)(32)–(ω-C11C5)(23) (ω-C47C51)(7)–(ω-C6C2)(6)
65	462	443.9	9.35		τ(C59—C10)(25)(ω-C59C55)(9) (δ-C59C55)(7) τ(C11—C43)(7)–(ω-C11C5)(7)–(τ′-R1)(5)–(δ-C47O52C51) (5)–τ(C59—C55)(5)
62	435		29.73		τ(C59—C9)(22)–(ω-C59C55)(11) (ρ-C51C47)(10) τ(C59—C10)(8) (ω-C11C5)(8) (δ-C59C55)(7)

Proposed assignment and potential energy distribution (PED) for vibrational modes: types of vibrations: ν – stretching, δ_{sc} – scissoring, ρ – rocking, ω – wagging, t – twisting, δ – deformation, δ_{as} – asymmetric deformation, τ – torsion. R1 – pyrrole ring and R2 – benzene ring.

the C—H bond upon complexation. It has further been claimed that contrary to standard H-bonds conventional H-bonds interactions are primarily governed by dispersion forces [46–49]. Other authors have arrived at the conclusion that C—H···O interactions should be considered as true H-bonds in spite of the shortening of the C—H bond upon complex formation. The assignment shows that methylene (CH_2) and methyl (CH_3) group associated with several vibrational modes, such as symmetric, asymmetric stretching, and scissoring, rocking, wagging, twisting, symmetric and asymmetric deformation. Three methyl groups are present in the molecule. Two of them are directly attached to the pyrrole ring and third is attached to the CH_2 of ester. They are abbreviated as Me2, Me3 and Me1 respectively. In second monomer unit of dimer, they are abbreviated as Me5, Me6 and Me4 respectively. The observed stretching vibration of ester methyl (Me1) at 2983 cm^{-1} is in agreement with the calculated wavenumber at 3017 cm^{-1}. The stretching vibration of pyrrole methyl (Me3) is observed at 2928 cm^{-1}, whereas this is calculated as 2937 cm^{-1}. Asymmetric deformations of Me3 are observed at 1480, 1430 cm^{-1}, whereas these are calculated at 1499, 1431 cm^{-1} respectively. Symmetric deformation of Me3 is observed at 1378 cm^{-1}, whereas this is calculated as 1382 cm^{-1}. The observed Me3-rocking at 1006 cm^{-1} agrees well with the calculated wavenumber at 1008 cm^{-1}. In the ECPADMPC the CH_2 (methylene) group is joined with C=O group and CH_3 group. This group gives characteristic stretching absorption below 3000 cm^{-1}. In FT-IR spectrum, the observed band at 1280 cm^{-1} is assigned to CH_2-wagging. The observed wagging at 1280 cm^{-1} corresponds to the calculated wavenumber at 1336 cm^{-1}. The aromatic structure shows the presence of C—H stretching vibration in the region 3100–3000 cm^{-1}, which is the characteristic region for the ready identification of C—H stretching vibration [50]. The C—H stretching vibration of benzene ring is observed at 3065 cm^{-1}. DFT calculations predict this band at 3172 cm^{-1}.

4.4.3. C=C vibrations

In aromatic hydrocarbon, skeletal vibrations involving carbon–carbon stretching within ring are absorbed in the region between 1600 and 1585 cm^{-1} [51]. The wavenumber calculated at 1592 cm^{-1} assigned to the C=C stretches in benzene ring. The calculated wavenumber at 1592 cm^{-1} assigned to the C=C stretching vibrational mode of Ar—C=C—C=O part of molecule.

4.4.4. C=O vibrations

The position of the carbonyl C=O stretching band is determine by the following factors: (1) the physical state, (2) electronic and mass effect of neighboring substituent, (3) conjugation, (4) hydrogen bonding (intermolecular and intramolecular), and (5) ring strain. Consideration of these factors leads to a considerable amount of information about the environment of the C=O group [51]. In general, C=O stretching vibrations of ester give rise to absorption band in the region of 1870–1540 cm^{-1}. In the FT-IR spectrum of ECPADMPC ester carbonyl (C=O) stretches are calculated at 1650 cm^{-1} in dimer, and 1689 cm^{-1} in monomer and the corresponding peak is observed at 1592 cm^{-1} in FT-IR spectrum. The observed $\nu_{C=O}$ absorption band at 1592 cm^{-1} agrees well with the calculated wavenumber of dimer at 1650 cm^{-1}. The C—O—C deformations mode of ester group is calculated at 1007, 868, 857, 776 and 772 cm^{-1}. The calculated —C—O—C— deformation mode at 1007 cm^{-1} agrees well with the wavenumber at 1006 cm^{-1} in the experimental IR-spectrum of ECPADMPC at cm^{-1}. Other modes of

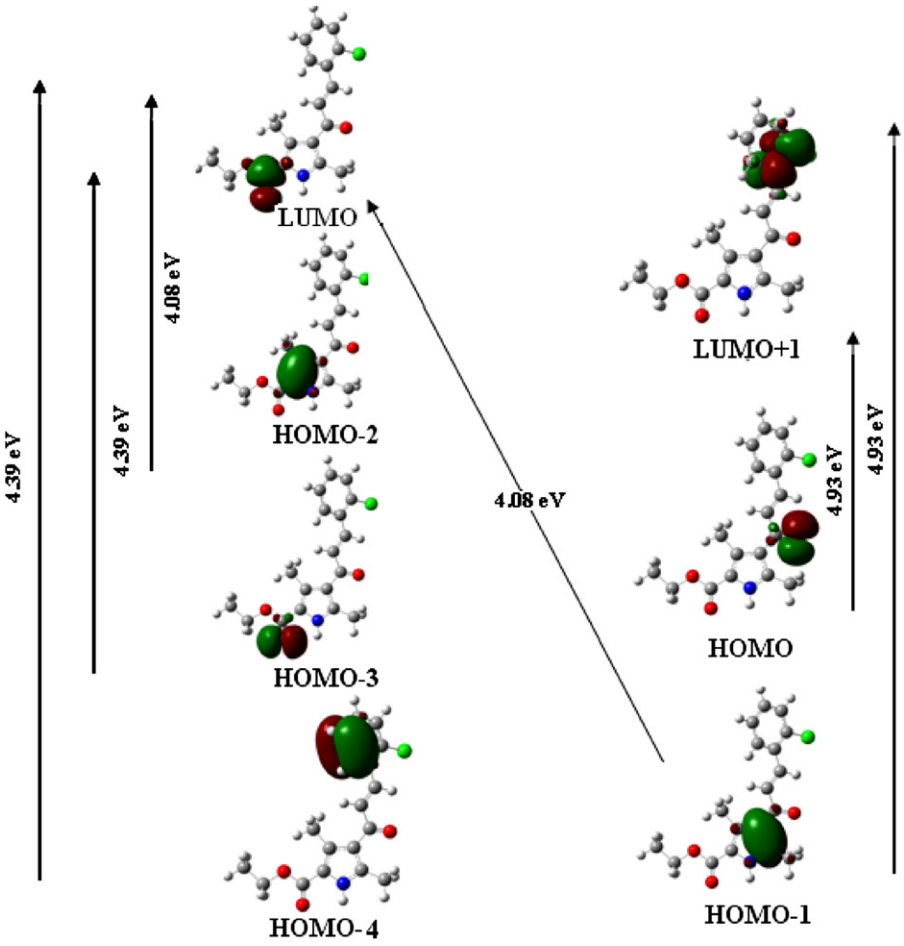

Fig. 8. The molecular orbitals of ECPADMPC at B3LYP/6-31G(d,p) level.

this C—O group vibration with combinations of other group modes and their corresponding contributions are given in Table 4.

The C=O carbonyl group of cyclic and acyclic moieties are generally observed at 1670–1820 cm^{-1}. The C=O carbonyl group present in chalcone frame Ar—C=C—C=O-py absorb at higher wavenumber than ester carbonyl. Conjugation with a double bond (>C=C<) results in delocalization of π electrons of the carbonyl group reduces the double bond character of the C—O bond, causing absorption at lower wavenumbers Hence conjugated C=O with others causes absorption in the 1685–1666 cm^{-1} region or slight reduced frequency. The stretching vibration of keto carbonyl group ($\nu_{C=O}$) calculated at 1689 cm^{-1} in monomer and 1687 cm^{-1} in dimer is corroborated well with the observed wavenumber at 1669 cm^{-1} in FT-IR spectrum of ECPADMPC.

4.4.5. C—Cl vibrations

The vibrations belonging to the bond between the aromatic ring and the halogen atoms (Ar—Cl) are worth to discuss, since mixing of vibrations is possible due to the lowering of the molecular symmetry [51,52]. The C—Cl stretching vibrations (ν_{C-Cl}) in chlorobenzenes

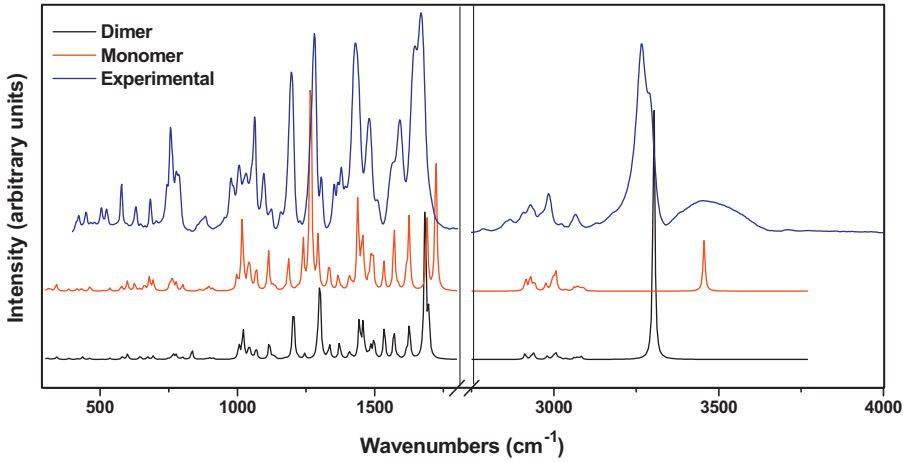

Fig. 9. The FT-IR spectrum (experimental and simulated) of the ECPADMPC.

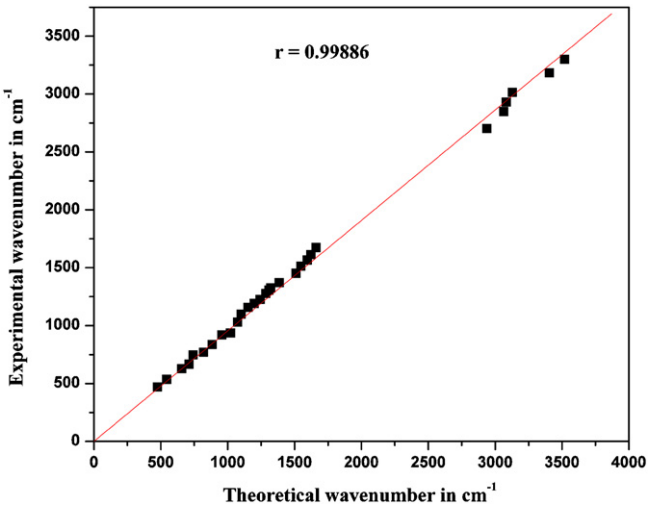

Fig. 10. The correlation graph between experimental and calculated (monomer and dimer) wavenumbers.

are observed in the region between 1096 and 1089 cm^{-1} [49]. Mooney [53,54] assigned vibrations of C—X group (X = Cl, Br, I) in the frequency range of 1129–480 cm^{-1}. In the FT-IR spectrum of title molecule, absorption band at 1063 cm^{-1} is assigned to C—Cl stretching vibrations. In dimer PED, ν_{C-Cl} calculated at 1012 cm^{-1} with 7% contribution.

4.5. AIM calculation

The dimer formation is due to two bifurcated H-bonds, one with O7 hydrogen accepting center and two hydrogen donating bonds N53—H56 and C59—H65; and another with O52 hydrogen accepting center and two hydrogen donating bonds N1—H24 and C11—H31. The both connections are related through the π-delocalization. In both intramolecular and intermolecular H-bonding π-electron delocalization effects are detectable and characterized with the use of the QTAIM methods. The decomposition scheme of the interaction energy is applied to expand the knowledge and the nature of RAHBs. The shorter proton–acceptor distance were detected indicating interactions are covalent. The Laplacien of electron density at the H—N···O bond critical point is negative, or at least the electron density at BCP is negative. The analysis of the interaction energy component shows that the delocalization energy terms is the most important attractive contribution. For hydrogen bonds covalent in nature, the delocalization interaction energy terms are the most important attractive contribution. Geometrical as well as topological parameters are useful tool to characterize the strength of hydrogen bond. The geometrical criteria for the existence of hydrogen bond are as follows: (i) The distance between proton (H) and acceptor (A) is less than the sum of their van der Waal's radii of these atoms. (ii) The 'donor (D)—proton (H)···acceptor (A)' angle is greater than 90°. (iii) The elongation of 'donor (D)—proton(H)' bond length is observed.

As the above criteria are frequently considered as insufficient, the existence of hydrogen bond could be supported further by Koch and Popelier criteria [55] based on 'Atoms in Molecules' theory (i) the existence of bond critical point for the 'proton (H)...acceptor (A)' contact as a confirmation of the existence of hydrogen bonding interaction. (ii) The value of electron density ($\rho_{H\cdots A}$) should be within the range 0.002–0.040 a.u. (iii) The corresponding Laplacian $^2\rho(r_{BCP})$ should be within the range 0.024–0.139 a.u. According to Rozas et al. [56] the interactions may be classified as follows: (i) strong H-bonds are characterized by $^2\rho_{(BCP)} < 0$ and $H_{BCP} < 0$ and their covalent character is established. (ii) Medium H-bonds are characterized by $^2\rho_{(BCP)} > 0$ and $H_{BCP} < 0$ and their partially covalent character is established. (iii) Weak H-bonds are characterized by $^2\rho_{(BCP)} > 0$ and $H_{BCP} > 0$ and they are mainly electrostatic. The weak interactions are characterized by $^2\rho_{(BCP)} > 0$ and $H_{BCP} > 0$ and the distance between interacting atoms is greater than the sum of van der Waal's radii of these atoms.

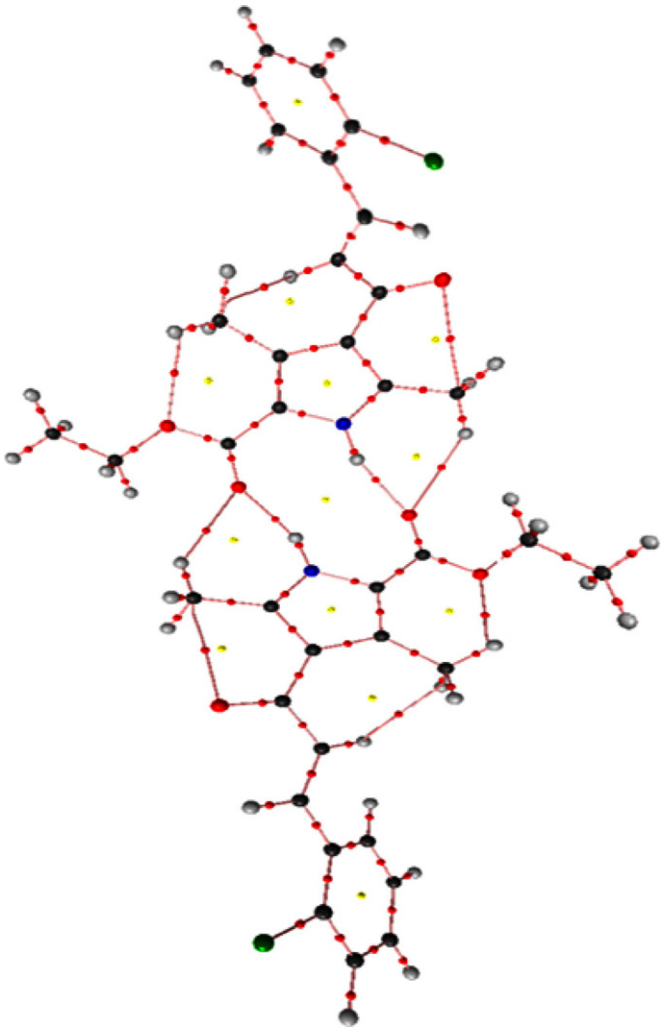

Fig. 11. Molecular graph of ECPADMPC at B3LYP/6-31G(d,p) level using AIM program: bond critical points (small red spheres), ring critical points (small yellow sphere), and bond paths (pink lines). (For interpretation of the references to color in this figure legend, the reader is referred to the web version of this article.)

Molecular graph of the dimer using AIM program at B3LYP/6-31G(d,p) level is shown in Fig. 11. The geometrical parameters for hydrogen bonds are given in Table 5. Geometrical as well as topological parameters for bonds of interacting atoms in dimer are given in Table 6. On the basis of these parameters, O52···H24, O7···H56 are weak hydrogen bonds and O44···H62, O8···H34, C11···O17, C59···O68, C12···H36, C58···H70, O7···H65, O52···H31are weak interactions. The various type of interactions visualized in molecular graph are classified on the basis of geometrical, topological

Table 5
Geometrical parameters for hydrogen bond in dimer: bond length (Å), bond angle (°).

N—H···O	N—H	H···O	N···O	N—H···O
N1—H24···O52	1.02	1.90	2.89	160.71
N53—H56···O7	1.02	1.90	2.89	160.70

Table 6
Geometrical parameters (bond length) and topological parameters for bonds of interacting atoms: electron density (ρ_{BCP}), Laplacian of electron density ($\nabla^2(\rho_{BCP})$), electron kinetic energy density (G_{BCP}), electron potential energy density (V_{BCP}), total electron energy density (H_{BCP}) at bond critical point (BCP) and estimated interaction energy (E_{int}).

Interactions	Bond length	$\rho_{(BCP)}$	$\nabla^2\rho_{(BCP)}$	G_{BCP}	V_{BCP}	H_{BCP}	E_{int}
O52···H24	1.9	0.03	0.08	0.02	−0.02	0.0005	−6.14
O7···H56	1.9	0.03	0.08	0.02	−0.02	0.0005	−6.14
O44···H62	2.32	0.01	0.05	0.01	−0.01	0.001	−3.26
O8···H34	2.32	0.01	0.05	0.01	−0.01	0.001	−3.265
C11···O17	2.89	0.01	0.05	0.01	−0.01	0.0015	−2.71
C59···O68	2.89	0.01	0.05	0.01	−0.01	0.0015	−2.71
C12···H36	2.56	0.01	0.04	0.01	−0.01	0.0024	−1.79
C58···H70	2.56	0.01	0.04	0.01	−0.01	0.0024	−1.79
O7···H65	2.6	0.01	0.03	0.01	−0	0.0009	−1.51
O52···H31	2.6	0.01	0.03	0.01	−0	0.0009	−1.5

$\rho_{(BCP)}$, $\nabla^2\rho_{(BCP)}$, G_{BCP}, V_{BCP}, H_{BCP} (in a.u.); E_{int} (kcal/mol).

and energetic parameters. In this article, the Bader's theory application is used to estimate hydrogen bond energy (E). Espinosa proposed proportionality between hydrogen bond energy (E) and potential energy density (V_{BCP}) at H···O contact: $E = 1/2(V_{BCP})$ [57]. According to AIM calculations, the binding energy of dimer is sum of the energies of all intermolecular interactions and this is calculated as −15.29 kcal/mol. The intermolecular hydrogen bond energy of dimer is sum of the energies of both heteronuclear intermolecular hydrogen bonds (N—H···O) and this is calculated as −12.28 kcal/mol.

There are several interacting effects such as dynamic disorder, orientational disorder and mesomeric effect connected with hydrogen bonding especially in crystal structures. The strength of H-bonds in dimmers is often result of the existence of such effect but may also be explained within the conditions related to the RAHB. In dimer often there is equalization of certain bonds, potential double movement of protons between electronegative atoms or regions of electron excess. In RAHBs model there is an effective mixing in two forms. The ellipticity (ε) at BCP is a sensitive index to monitor the π-character of bond. The ε is related to λ_1 and λ_2, which correspond to the eigen values of Hessian and defined by a relationship: $\varepsilon = (\lambda_1/\lambda_2) - 1$. The dimer has sixteen-memberd pseudo ring which contains two hydrogen bonds N1H24···O52 and N53H56···O7 as well as other bonds O7C6, C6C2, C2C3, C3C4, C4C5, C5N1, O52C47, C47C51, C51C54, C54C57, C57C55, C55—N53 for which ellipticity values are 0.1006, 0.2251, 0.2865, 0.2105, 0.2498, 0.1483, 0.1006, 0.2251, 0.2865, 0.2105, 0.2498, 0.1483 respectively. These values of ε are corresponds to the aromatic bonds reported in literature [58]. This confirms the presence of resonance assisted hydrogen bonds because both N and O atoms are interconnected by a system of appropriate electron density.

4.6. Chemical reactivity

4.6.1. Global reactivity descriptors

The energies of frontier molecular orbitals (ε_{HOMO}, ε_{LUMO}), energy band gap ($\varepsilon_{HOMO} - \varepsilon_{LUMO}$), electronegativity ($\chi$), chemical potential ($\mu$), global hardness ($\eta$), global softness ($S$) and global electrophilicity index (ω) [59–63] of ECPADMPC have been listed in Table 7. On the basis of ε_{HOMO}, ε_{LUMO} these are calculated using Eqs. (1)–(5) given below:

$$\chi = -\frac{1}{2}(\varepsilon_{LUMO} + \varepsilon_{HOMO}) \quad (1)$$

$$\mu = -\chi = \frac{1}{2}(\varepsilon_{LUMO} + \varepsilon_{HOMO}) \quad (2)$$

$$\eta = \frac{1}{2}(\varepsilon_{LUMO} - \varepsilon_{HOMO}) \quad (3)$$

$$S = \frac{1}{2\eta} \quad (4)$$

$$\omega = \frac{\mu^2}{2\eta} \quad (5)$$

Electrophilic charge transfer (ECT) [59] is defined as the difference between the ΔN_{max} values of interacting molecules. For two molecules I and II approaching each other (i) if ECT > 0, charge flows from II to I and (ii) if ECT < 0, charge flows from I to II. ECT is calculated using Eq. (6):

$$ECT = (\Delta N_{max})_I - (\Delta N_{max})_{II} \quad (6)$$

where $(\Delta N_{max})_I = -\mu_I/\eta_I$ and $(\Delta N_{max})_{II} = -\mu_{II}/\eta_{II}$.

The calculated value of ECT < 0 (−0.48385 eV), for reactant molecules ethyl 4-acetyl-3,5-dimethyl-1*H*-pyrrole-2-carboxylate (A) and 2-chlorobenzaldehyde (B) indicates charge flow from A to B. Therefore, A acts as electron donor and B as electron acceptor. The high value of chemical potential and low value of electrophilicity index for A also favor its nucleophilic behavior. In the same way, the low value of chemical potential and high value of electrophilicity index for B favor its electrophilic behavior.

4.6.2. Local reactivity descriptors

Using Hirshfeld atomic charges of neutral, cation and anion state of ECPADMPC, Fukui functions (f_k^+, f_k^-, f_k^0), local softnesses (s_k^+, s_k^-, s_k^0) and local electrophilicity indices (ω_k^+, ω_k^-, ω_k^0) [60,63]. Fukui Functions are calculated using the following equations (7)–(9).

$$f_k^+ = [q(N+1) - q(N)] \quad \text{for nucleophilic attack} \quad (7)$$

$$f_k^- = [q(N) - q(N-1)] \quad \text{for electrophilic attack} \quad (8)$$

$$f_k^0 = \frac{1}{2}[q(N+1) + q(N-1)] \quad \text{for radical attack} \quad (9)$$

Local softnesses and electrophilicity indices are calculated using Eqs. (10) and (11).

$$s_k^+ = Sf_k^+, s_k^- = Sf_k^-, s_k^0 = Sf_k^0, \quad (10)$$

$$\omega_k^+ = \omega f_k^+, \omega_k^- = \omega f_k^-, \omega_k^- = \omega f_k^-, \quad (11)$$

where +, −, 0 signs show nucleophilic, electrophilic and radical attack respectively.

Fukui functions, local softnesses and local electrophilicity indices for selected atomic sites in ECPADMPC have been listed in Table 8. The maximum values of all the three local electrophilic reactivity descriptors (f_k^+, s_k^+, ω_k^+) at C15 indicate that this site is prone to nucleophilic attack. The calculated local reactivity descriptors for synthesized molecule favor the formation of new

Table 7
Calculated ε_{HOMO}, ε_{LUMO}, energy band gap ($\varepsilon_H - \varepsilon_L$), chemical potential ($\mu$), electronegativity ($\chi$), global hardness ($\eta$), global softness ($S$) and global electrophilicity index (ω) for A, B and C at B3LYP/6-31G(d,p) level.

Molecule	ε_{HOMO}	ε_{LUMO}	$\varepsilon_H - \varepsilon_L$	μ	χ	η	S	ω
Reactant (A)	−6.03	−0.82	−5.22	−3.42	3.42	2.61	0.19	2.25
Reactant (B)	−7.10	−2.02	−5.08	−4.56	4.56	2.54	0.197	4.10
Product (C)	−6.00	−1.97	−4.03	−3.99	3.99	2.01	0.25	3.95

ε_{homo}, ε_{lumo}, $\varepsilon_H - \varepsilon_L$, μ, χ, η, ω (in eV); S (in eV^{-1}).

Table 8
Fukui functions (f_k^+, f_k^-/eV), local softnesses (s_k^+, s_k^-/eV^{-1}), local electrophilicity indices (ω_k^+, ω_k^-/eV) for selected atomic sites of ECPADMPC, using Mulliken population analysis at B3LYP/6-31G(d,p) level.

Product (C)	f_k^+	f_k^-	s_k^+	s_k^-	ω_k^+	ω_k^-
C6	20.87	19.73	37.94	35.86	1.72	1.63
C13	30.45	8.81	55.34	16.00	2.52	0.73
C14	22.19	9.51	40.33	17.28	1.83	0.79
C15	42.46	18.11	77.21	32.92	3.51	1.50

heterocyclic compounds such as pyrazoline and oxazoline by nucleophilic attack on the C15 site of C14—C15 bond.

5. Conclusions

ECPADMPC is synthesized and characterized by ^{1}H NMR, UV–Vis, FT-IR, Mass and elemental analysis. The calculated ^{1}H NMR and ^{13}C NMR chemical shifts using gauge including atomic orbitals (GIAO) approach are in good agreement with the observed chemical shifts experimentally. Theoretical electronic absorption spectra show both blue shift and red shift compared with the experimental data. The molecular orbital coefficients analyses suggest that electronic transitions are assigned to $\pi \rightarrow \pi^*$ and $n \rightarrow \pi^*$ in nature. In the present study, experimental and calculated vibrational wavenumber analysis confirms the existence of dimer by involvement of heteronuclear association through pyrrolic (N—H) and carbonyl (C═O) oxygen of ester. The calculated binding energies of dimer using both DFT and AIM theories are −13.92 and −15.29 kcal/mol respectively. AIM theory is more appropriate than DFT theory since this is also applicable to calculate the intermolecular hydrogen bond energy of dimer and this is calculated as −12.28 kcal/mol. The results of AIM ellipticity confirm the existence of resonance assisted intermolecular hydrogen bonds in dimer. In addition, theoretical results from reactivity descriptors show that C15 is more reactive site for nucleophilic attack.

Acknowledgments

The authors are thankful to the Directors of IIT Kanpur and CDRI Lucknow for providing spectral measurements of the compound and the CSIR New Delhi for financial supports.

Appendix A. Supplementary data

Supplementary data associated with this article can be found, in the online version, at http://dx.doi.org/10.1016/j.saa.2012.03.059.

References

[1] B.C. Patil, S.K. Mahajan, A.K. Suvarna, Pharm. Sci. Res. J. 3 (2009) 11–22.
[2] H. Aichaoui, F. Guenadil, C.N. Kapanda, D.M. Lambert, E. Christopher, R. McCurdy, E. Jacques, H. Poupaert, Med. Chem. Res. 18 (2009) 467–476.
[3] S.K. Awasthi, N. Mishra, B. Kumar, M. Sharma, A. Bhattacharya, L.C. Mishra, V.K. Bhasin, Med. Chem. Res. 18 (2009) 407–420.
[4] S.S Lim, H.S. Kim, D.U Lee, Bull. Korean Chem. Soc. 28 (2007) 2495–2497.
[5] E. Szliszka, Z.P. Czuba, B. Mazur, L. Sedek, A. Paradysz, W. Krol, Int. J. Mol. Sci. 11 (2010) 1–13.
[6] C. Echeverria, J.F. Santibanez, O. Donoso-Tauda, C.A. Escobar, R.R. Tagle, Int. J. Mol. Sci. 10 (2009) 221–231.
[7] F. Lunardi, M. Guzela, A.T. Rodrigues, R. Corre, I.M. Eger-Mangrich, Steindel, E.C. Grisard, J. Assreuy, J.B. Calixto, A.R.S Santos, Antimicrob. Agents Chemother. 47 (2003) 1449–1451.
[8] H.L. Yadav, P. Gupta, P.S. Pawar, P.K. Singour, U.K. Patil, Med. Chem. Res. 19 (2010) 1–8.
[9] X.W. Zhang, D.H. Zhao, Y.C. Quan, L.P. Sun, X.M. Yin, L.P. Guan, Med. Chem. Res. 19 (2010) 403–412.
[10] N.M. Bhatia, K.R. Mahadik, M.S. Bhatia, Chem. Pap. 63 (2009) 456–463.
[11] S.K. Awasthi, N. Mishra, S.K. Dixit, A. Singh, M. Yadav, S.S. Yadav, S. Rathaur, Am. J. Trop. Med. Hyg. 80 (2009) 764–768.
[12] K.L. Lahtchev, D.I. Batovska, S.P. Parushev, V.M. Ubiyvovk, A.A. Sibirny, Eur. J. Med. Chem. 43 (2008) 2220–2228.
[13] N. Yayli, O. Ucuncu, A. Yasar, M. Kucuk, E. Akyuz, S.A. Karaoglu, Turk. J. Chem. 30 (2006) 505–514.
[14] N.A. Begum, N. Roy, R.A. Laskar, K. Roy, Med. Chem. Res. 19 (2010) 1–14.
[15] S. Kaushik, N. Kumar, S. Drabu, Pharm. Res. 3 (2010) 257–262.
[16] P.M. Sivakumar, P.K. Prabhakar, M. Doble, Med. Chem. Res. 19 (2010) 1–17.
[17] R. Romagnoli, P.G. Baraldi, M.D. Carrion, C.L. Cara, O. Cruz-Lopez, D. Preti, Bioorg. Med. Chem. 16 (2008) 5367–5376.
[18] M. Najafian, A. Ebrahim-Habibi, N. Hezareh, P. Yaghmaei, K. Parivar, B. Larijani, Mol. Biol. Rep. 10 (2010) 271–274.
[19] A. Zarghi, T. Zebardast, F. Hakimion, F.H. Shirazi, P.N.P. Rao, E.E. Knaus, Bioorg. Med. Chem. 14 (2006) 7044–7050.
[20] F. Chimenti, R. Fioravanti, A. Bolasco, P. Chimenti, D. Secci, F. Rossi, M. Yanez, O.F. Francisco, F. Ortuso, S. Alcaro, J. Med. Chem. 10 (2009) 1–8.
[21] F.A. Tarek, Chem. Phys. 324 (2006) 631–638.
[22] D. Millán, M. Domínguez, M.C. Rezende, Dyes Pigments 77 (2008) 441–445.
[23] L. Mager, C. Melzer, M. Barzoukas, A. Fort, S. Mery, J.F. Nicoud, Appl. Phys. Lett. 71 (1997) 2248–2250.
[24] B. Gu, W. Ji, P.S. Patil, S.M. Dharmaprakash, J. Appl. Phys. 103 (2008) 103511–103516.
[25] M.P. Cockerham, C.C. Frazier, S. Guha, E.A. Chauchard, Appl. Phys. B 53 (1991) 275–278.
[26] H. Forejtníková, K. Lunerová, R. Kubínová, D. Jankovská, R. Marek, R. Kareš, V. Suchý, J. Vondráček, M. Machala, Toxicology 208 (2005) 81–93.
[27] R.F.W. Bader, Atoms in Molecules. A Quantum Theory, Oxford University Press, Oxford, 1990.
[28] L. Sobczyk, S.J. Grabowski, T.M. Krygowski, Chem. Rev. 105 (2005) 3513–3560.
[29] M. Jablonski, M. Palusiak, J. Phys. Chem. A 114 (2010) 2240–2244.
[30] A.I. Vogel, Practical Organic Chemistry, Prentice Hall Publication, New York, 1956, p. 344.
[31] E.J.H. Chu, T.C. Chu, J. Org. Chem. 19 (1954) 266–269.
[32] M.J. Frisch, et al., Gaussian 03, Revision C.01, Gaussian Inc., Wallingford, CT, 2004.
[33] A.D. Becke, J. Chem. Phys. 98 (1993) 5648–5652.
[34] C.T. Lee, W.T. Yang, R.G.B. Parr, Phys. Rev. 37 (1988) 785–790.
[35] K. Wolinski, J.F. Hinton, J.F. Pulay, J. Am. Chem. Soc. 112 (1990) 8251–8260.
[36] N. Sundaraganesan, E. Kavitha, S. Sebastian, J.P. Cornard, M. Martel, Spectrochim. Acta A 74 (2009) 788–797.
[37] J.M.L. Martin, V. Alsenoy, C.V. Alsenoy, Gar2ped, University of Antwerp, 1995.
[38] P. Pulay, G. Fogarasi, F. Pang, J.E. Boggs, J. Am. Chem. Soc. 101 (1979) 2550–2560.
[39] G.A. Zhurko, D.A. Zhurko, Chemcraft: lite version build 08 (freeware), 2005.
[40] Computer program Gauss View 0.3, Ver. 2, Gaussian Inc., Pittsburgh, PA.
[41] R.F.W. Bader, J.R. Cheeseman, AIMPAC, 2000.
[42] C.T. Arranja, M.R. Silva, A.M. Beja, A.F.P.V. Ferreira, A.J.F.N. Sobral, Acta Crystallogr. E 64 (2008) o1989.
[43] M.G. Gardiner, R.C. Jones, S. Ng, J.A. Smith, Acta Crystallogr. E63 (2007) o470.
[44] M.C. Etter, Acc. Chem. Res. 23 (1990) 120–126.
[45] S.F. Boys, F. Bernardi, Mol. Phys. 19 (1970) 553–556.
[46] A.T. Dubis, S.J. Grabowski, D.B. Romanowska, T. Misiaszek, J. Leszczynski, J. Phys. Chem. A 106 (2002) 10613–10621.
[47] Jorly Joseph, E.D. Jemmis, J. Am. Chem. Soc. 129 (2007) 4620–4632.
[48] S.J. Grabowski, Chem. Phys. Lett. 388 (2001) 361–366.
[49] S.J. Grabowski, J. Phys. Chem. A 105 (2001) 10739–10746.
[50] S.J. Grabowski, J. Mol. Struct. 562 (2001) 137–143.
[51] R.M. Silverstein, F.X. Webster, Spectrometric Identification of Organic Compounds, 6th Edition, Jon Wiley Sons Inc., New York, 1963.
[52] R.A. Yadav, I.S. Singh, Indian J. Pure Appl. Phys. 23 (1985) 626–627.
[53] E.F. Mooney, Spectrochim. Acta A 20 (1964) 1021–1032.
[54] E.F. Mooney, Spectrochim. Acta A 19 (1963) 877–887.

[55] U. Koch, P. Popelier, J. Phys. Chem. A 99 (1995) 9747–9754.
[56] I. Rozas, I. Alkorta, J. Elguero, J. Am. Chem. Soc. 122 (2000) 11154–11161.
[57] E. Espinosa, E. Molins, C. Lecomte, Chem. Phys. Lett. 285 (1998) 170–173.
[58] I.F. Matta, R.J. Boyd, An Introduction to the Quantum Theory of Atoms in Molecules, Wiley-VCH Verlag Gmbh, 2007.
[59] R.G. Pearson, J. Org. Chem. 54 (1989) 1430–1432.
[60] P. Geerlings, F.D. Proft, W. Langenaeker, Chem. Rev. 103 (2003) 1793–1873.
[61] R.G. Parr, L.V. Szentpály, S. Liu, J. Am. Chem. Soc. 121 (1999) 1922–1924.
[62] P.K. Chattaraj, S. Giri, J. Phys. Chem. A 111 (2007) 11116–11121.
[63] J. Padmanabhan, R. Parthasarathi, V. Subramaniaan, P.K. Chattaraj, J. Phys. Chem. A 111 (2007) 1358–1361.